

NASA  
TP  
1128  
c.1

NASA Technical Paper 1128

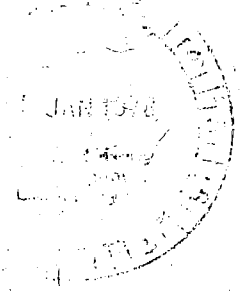
TECH LIBRARY KAFB, NM  
0134515

LOAN COPY? RE  
AFWL TECHNICAL  
KIRTLAND AFB

# Friction and Wear of Several Compressor Gas-Path Seal Materials

Robert C. Bill and Donald W. Wisander

JANUARY 1978





NASA Technical Paper 1128

# Friction and Wear of Several Compressor Gas-Path Seal Materials

Robert C. Bill  
Propulsion Laboratory  
U.S. Army R&T Laboratories (AVRADCOM)

and

Donald W. Wisander  
Lewis Research Center  
Cleveland, Ohio



National Aeronautics  
and Space Administration

**Scientific and Technical  
Information Office**

1978

# FRICITION AND WEAR OF SEVERAL COMPRESSOR GAS-PATH SEAL MATERIALS

by Robert C. Bill\* and Donald W. Wisander

Lewis Research Center

## SUMMARY

Rub interaction experiments were conducted on a series of sintered and plasma-sprayed gas-path seal materials. Both blade-tip and labyrinth seal knife-edge rotor geometries were used. In all cases, the rotor was made of Ti-6Al-4V. Rotor speeds of up to 115 meters per second and radial incursion rates of  $25.4 \times 10^{-6}$  and  $254 \times 10^{-6}$  meter per second were employed.

The most rub tolerant materials based on observed rotor wear and frictional behavior were sintered Nichrome (~40 percent dense) and plasma-sprayed nickel - 25 percent graphite. It was also found that the radial and frictional loads encountered during rub interaction experiments with dense plasma-sprayed aluminum could be significantly reduced by providing a soft compliant backing for the aluminum.

In general, it was observed that rotor wear and high frictional energy generation rates accompanied smearing or surface densification of the materials investigated. The onset of smearing was sensitive to rub interaction parameters and seal geometry. Two complementary models are proposed to account for the smearing trends. One is based on thermal effects, the other on particulate escape effects. They are shown to be consistent with the experimental evidence at hand. Together they predict that smearing, with the onset of high frictional rub energy conditions, is favored when incursion rates (radial motion) are low, incursion depths are high, the seal geometry is of a knife-edge (continuous surface) character, and the seal material particle size is small.

## INTRODUCTION

The efficiency of gas turbine engines is strongly dependent on clearances between stationary gas-path seal components and rotating blade tips or labyrinth seal knife edges. Very significant reductions in thrust specific fuel consumption are realizable if minimum gas-path seal clearances are maintained throughout the engine (refs.

---

\*Propulsion Laboratory, U. S. Army R&T Laboratories (AVRADCOM).

1 and 2). Operating with minimal clearances inevitably results in rubs between the rotating and stationary components. Such rubs, occurring as they do at extremely high speeds (typically 300 to 400 m/sec), can result in destructively high temperatures, wear to the rotating components, and unpredictable behavior of the gas-path seal material comprising the static component.

From the standpoints of maintaining engine efficiency and structural integrity, it is desired that wear to the static component (gas-path seal material) occur rather than wear to the rotating component. Gas-path seal materials are designed and structured so as to preferentially undergo wear, thus minimizing wear to the rotating component in the event of a rub interaction. Generically there are three types of gas-path seal material systems employed in a gas turbine engine. First there are those that may be characterized as low density (60 to 80 percent porosity range) metallic types, often sintered. Such materials accommodate rub interactions by virtue of their friable nature. The discrete particles are knocked off the seal surface by the rotor. Depending on composition, these materials are used in hot or cold section locations of gas turbine engines.

A second class of gas-path seal materials includes more dense structures (less than 30 percent porosity) which are often plasma-sprayed and, in some cases, sintered, hot pressed, or even cast. Rub interactions for this class of seal materials are accommodated in a more complex manner than were those for the first type of seal material. Usually a combination of plastic deformation, material compliance (densification), and machining mechanisms is involved. Again, variations of this type of material are used in gas-path seal locations throughout the engine - elastomeric materials being employed in low pressure compressor positions, low temperature metals in higher compressor stages, and high temperature materials in the turbine.

The third class of gas-path seal materials derives its rub tolerance from the geometric arrangement of thin metal sheets from which the seal is fabricated. Probably the most widely used example of this type is metallic honeycomb. The honeycomb cell walls are oriented in the radial direction. Consequently, very little metal to metal contact surface area is involved when a rub interaction occurs. Honeycomb structures are generally applied to low pressure turbine seal positions.

In this report, predictive models are proposed that describe the rub behavior of some compressor gas-path seal materials. In particular, these models describe how transitions from a relatively mild, low friction energy mode of rub interaction to a more severe mode involving much higher frictional energy occur. Experimental data are presented and correlated with the models. The experimental data include radial and frictional force measurements, rotor temperature measurements, wear to the rotating components, and microscopic observations of the seal material, rotor rub surface, and debris resulting from the rub interaction. Experiments were performed

using blade-tip and labyrinth seal knife-edge rotor configurations and rotational speeds to 115 meters per second. Radial "feedrates" - henceforth to be called incursion rates - were varied; values of  $25.4 \times 10^{-6}$  and  $254 \times 10^{-6}$  meter per second were used.

## APPARATUS

Rub evaluations were conducted on the apparatus shown in figure 1. Either a simulated labyrinth seal knife edge as shown in the inset of figure 1 or a complement of 12 simulated blade tips as shown in the rig schematic of figure 1 were rotated at speeds to 115 meters per second. Drive power was provided by a 2.24-kilowatt induction motor coupled to a continuous speed variator, thus permitting control of the rub speed.

Simulated blade-tip specimens were 3.175 millimeters thick and 12.7 millimeters wide. The knife-edge geometry was of a rectangular radial section with a 0.508-millimeter knife-edge thickness. The rotor diameter was 19.1 centimeters for both geometries.

The gas-path seal material sample was mounted on a slideway feed mechanism so that it could be driven radially into the rotor. Radial incursion rates of  $25.4 \times 10^{-6}$  and  $254 \times 10^{-6}$  meter per second were employed.

During a rub interaction test, radial loads and frictional torque were continuously recorded, and an infrared pyrometer was used to monitor and record the blade tip or knife edge temperature. Radial loads were sensed by means of strain gages applied to the gas-path seal material sample support. A torque transducer in the shaft system, located between the speed variator and the bearing spindle directly behind the disk, provided frictional torque data. The infrared pyrometer, located  $90^\circ$  past the rub contact as shown in figure 1, indicated the number of blade tips or the number of discrete locations on the knife edge participating in the rub interaction per revolution as well as providing a temperature indication.

Wear debris generated during the rub interaction was collected on the fixture indicated in figure 1. Debris particles impinged a strip of sticky tape and thus were captured for subsequent examination and evaluation. Optical microscopy, SEM, and EDAX were used to study the rub debris.

A dial gage indicator showed the relative radial motion of the feed slideway carriage with respect to the rotating disk. Interaction depths could be controlled to within 25 micrometers of the desired depth. Usually 750-micrometer incursion depths were employed.

## PROCEDURE

Prior to testing, the blade tips were ground so that the tip surface was as nearly parallel as possible to the supporting root. The tip surface finish was about  $0.5 \times 10^{-6}$  meter (20  $\mu$ in. rms) after conditioning. The tips were then cleaned with ethanol, and the height of each simulated blade tip was measured. Height variations were maintained to within  $\pm 4$  micrometers.

For the knife-edge seal geometries, the knife edge was machined in-situ so that the maximum radial runout was  $\pm 2.54 \times 10^{-6}$  meter. After machining the surface was honed (again, in-situ) using a SiC abrasive block and then rinsed with absolute ethanol.

Selected gas-path seal material samples were epoxy bonded to a mild steel backing which was screwed to a combination specimen support/cantilever load cell. The rotor was brought to the desired rotating speed, the selected incursion rate was set, and the rub interaction was initiated. In these tests the interaction was continued to a 750-micrometer depth.

Rotational speeds of 57 and 115 meters per second were selected for this study. The incursion rates employed were  $25.4 \times 10^{-6}$  and  $254 \times 10^{-6}$  meter per second.

A posttest evaluation included blade-tip and abradable material rub surface microscopic examination and wear debris examination. A measure of the wear (or transfer) to the blade-tip leading edges was obtained by observing specimen focus plane height changes over the tip surface during microscopic examination. Knife-edge wear was evaluated by means of circumferential profile traces taken before and after tests; these traces indicate changes in the radial dimension due to wear of the knife edge or transfer of the seal material to the knife edge.

## MATERIALS

Blade tips and labyrinth seal knife edges were fabricated from the Ti-6Al-4V alloy in the solution treated, age hardened condition (hardness was  $R_c 32$ ). This particular alloy is representative of materials used for compressor blades and labyrinth seal components in current gas turbine engines.

Five gas-path seal materials were evaluated in the blade-tip and knife-edge test configurations. A sintered Nichrome material, approximately 40 percent dense (60 percent porosity), served as a standard of abradability. The sintered particles comprising this material were about 75 to 100 micrometers in diameter, and the tensile strength was about  $4 \times 10^6$  newtons per square meter (600 psi).

Two density levels (19 and 21.5 percent) of sintered Hastelloy-X fibermetal, which is representative of compressor seal materials currently used in some engine

locations, were evaluated. Both of these materials were made of metal fibers typically 100 to 150 micrometers in length and 10 micrometers in diameter. The strength level of the 19 percent dense material was about  $10 \times 10^6$  newtons per meter (1500 psi), and the tensile strength of the 21.5 percent dense material was about  $12 \times 10^6$  newtons per square meter (1800 psi).

In addition to the sintered materials, three thermal-sprayed seal materials were evaluated. One was plasma-sprayed nickel - 25 volume percent graphite; it was sprayed to an approximate hardness of  $(R15_y)40 \pm 10$ . Flame-sprayed Nichrome - 7 volume percent boron nitride with a hardness of  $(R15_y)45 \pm 5$  was also evaluated. Finally, a dense plasma-sprayed aluminum coating was assessed as a gas-path seal material. All of these sprayed materials are employed in various gas-path seal locations. In addition, a 500-micrometer-thick layer of plasma-sprayed aluminum was applied to a 15-percent dense nickel - fibermetal substrate as an experimental concept to evaluate the efficacy of providing a compliant support to a dense seal material coating.

## RESULTS AND DISCUSSION

Experimental observations and measurements from the rub tests are presented first; these are followed by theoretical treatments of the various observed rub mechanisms. Models predicting how transitions from low frictional energy generation rate rub modes to high energy modes can occur are then developed. The theoretical treatments and modeling are shown to be consistent with experimentally observed rub phenomena and trends.

### Rub Test Results

Blade-tip tests. - The frictional and radial load patterns, the condition of the seal material rub surface after a test, and the visible thermal effects observed during testing are summarized in table I for each material and test condition. Peak radial and frictional load measurements are summarized in figures 2(a) and (b), respectively. Blade-tip wear and/or transfer measurements are also summarized in figure 2(a).

By way of explanation for table I, load patterns (both frictional and radial) are described as consisting of distinct events, continuous loading, or a combination of continuous loading with distinct events superimposed. Continuous loading characterizes a situation in which the radial and frictional loads are fairly steady throughout a rub test. Distinct events are short-term load bursts lasting from 0.1 to 1 second. Rub surfaces are described in table I as having been smeared, cleanly abraded, or torn. A smeared

rub surface consists of a continuous layer of plastically deformed material as opposed to the porous, or particulate, nature of the bulk material structure. In contrast, a cleanly abraded rub surface maintains the distinctly particulate, porous nature of the bulk material. A rub surface showing cracks transversely oriented with respect to the sliding direction, propagating obliquely into the seal material, is described as showing frictional tearing.

Very low blade-tip wear occurred for the 40-percent-dense sintered Nichrome and plasma-sprayed nickel graphite; the lowest radial and frictional loads were observed for these materials as shown in figure 2. Significant temperature peaks could not be detected on the blade tips, and only occasional yellow sparking took place during experiments on these materials. Very little smearing or surface densification was found to have taken place on the seal material rub surfaces. The discontinuous nature of the load pattern, as noted in table I for these materials, is thought to be due to a "self-erosion" effect. When a contact event occurs, the loose seal material particles generated promote further wear to the rub surface; consequently, clearances develop between the rotor and seal material. Another event can occur only after the seal material sample has been moved far enough radially to cause contact again.

Nineteen-percent-dense sintered Hastelloy-X fibermetal was observed to transfer to the blade tips with no measurable tip wear taking place. Both radial and frictional loads were higher than those measured for the sintered Nichrome and sprayed nickel graphite. Significant temperature peaks indicating bulk blade-tip temperature rises of  $200^{\circ}\text{C}$  under the pyrometer were seen for the 115 meter per second rub conditions; temperature rises of  $350^{\circ}\text{C}$  were seen under high incursion rate ( $254 \times 10^{-6}$  m/sec) conditions at 57 meters per second. Smearing over 20 to 40 percent of the rub surface was seen after rubbing with a  $25.4 \times 10^{-6}$  meter per second incursion rate under both tip speed conditions. Tearing of the rub surface resulted from high incursion rate test conditions; intermittent white sparking was observed during all tests.

Consistently higher blade-tip wear, compared to sintered Nichrome, resulted from rub interactions with 21.5-percent-dense Hastelloy-X fibermetal. Depending on the rub conditions, the radial and frictional loads were from 3 to 10 times greater than those loads measured for sintered Nichrome. Tests conducted at 115 meters per second were characterized by a semicontinuous intense white incandescence in the rub zone and by visible migratory glowing of the seal material contact surface. Temperature peaks in excess of  $350^{\circ}\text{C}$  were detected under the high speed rub conditions; almost total smearing of the seal material and heat discoloration were seen after the test. Considerably less smearing and heat discoloration of the fibermetal resulted from the 57 meter per second test.

Results from blade-tip rub interaction tests with plasma-sprayed Nichrome - boron nitride were generally similar to those obtained for the 21.5-percent-dense



Hastelloy-X fibermetal. In addition to seal material rub surface smearing, evidence of thermal shock damage was seen in the form of occasional blistering and cracking in the rub surface.

Dense, plasma-sprayed aluminum and a 500-micrometer coating of aluminum applied to a 15-percent-dense fibermetal substrate were evaluated at a 115 meter per second tip speed and  $25.4 \times 10^{-6}$  meter per second incursion rate. Radial and frictional loads for the dense aluminum coating were quite high, the frictional force being about 10 times that of sintered Nichrome. Very heavy transfer of aluminum to the Ti-6-4 blade tips was also observed, some tips being nearly completely capped. Blade-tip temperature rises of 240 Celsius degrees were indicated under the pyrometer with three to four blade tips simultaneously interacting. Applying the aluminum coating to a compliant substrate (15-percent-dense fibermetal) reduced frictional and radial loads by slightly more than 50 percent. Tip temperatures and aluminum transfer to the blade tips were not significantly reduced, however. The thin coating remained intact and adherent to the substrate after the rub interaction.

A common observation for all of the blade-tip rub tests is the occurrence of maximum radial and frictional loads under the high incursion rate condition (fig. 2). Also, load patterns tended to be more continuous - that is, events lasted longer - under high incursion rate conditions. Maximum blade tip wear, however, usually took place under the 115 meter per second rotational speed condition. The following sections will treat these observations in more detail.

Knife-edge seal tests. - Frictional and radial load patterns, condition of the seal material rub surface after a test, and visible thermal effects observed during testing are summarized in table I for each material subjected to knife-edge seal interaction. Peak radial and frictional loads are summarized in figure 3 along with knife-edge wear and/or transfer measurements.

Friction and wear results for the knife-edge seal tests (see fig. 3), like those for the blade-tip tests, showed the lowest frictional and radial loads for the 40-percent-dense sintered Nichrome. Transferred seal material, 3 to 5 micrometers (0.1 to 0.2 mil) high, was found over most of the knife edge after the test. There were isolated wear spots about 2 micrometers (0.1 mil) deep over less than 10 percent of the surface. The rub surface was seen to be smeared with brown heat discoloration of the seal material. The load pattern was characterized as a sequence of distinct events.

Plasma-sprayed nickel - 25 percent graphite showed frictional loads about twice as high as those of sintered Nichrome and a radial load about five times that of sintered Nichrome. Seven to 10 micrometers of transfer were seen over 70 percent of the knife edge and 3 to 5 micrometers of wear over 20 to 30 percent. As for the sintered Nichrome, the load pattern consisted of a sequence of distinct events with rub surface smearing being observed after the test.

There was little difference between the performance of the 19- and 21.5-percent-dense Hastelloy-X fibermetals. Both materials showed frictional and radial loads 50 to 100 percent greater than those for sintered Nichrome; this was probably due to the higher strength level of the fibermetal materials. Seal material transfer to the knife edge was observed to be very similar to that for the 40-percent-dense sintered Nichrome with isolated spots of wear again seen.

Very high friction and comparatively heavy transfer (5 to 10  $\mu\text{m}$ ) over most of the knife edge (a 17-4 PH steel knife edge was used in this case) accompanied rub tests against plasma-sprayed aluminum. Providing a compliant substrate in the form of 15-percent-dense nickel fibermetal resulted in significant radial and frictional load reduction but little difference in the observed transfer of aluminum to the knife edge (again, a 17-4 PH steel knife edge). Plasma-sprayed aluminum graphite showed a considerable reduction in radial and frictional loads compared to pure aluminum; however, some knife-edge wear occurred (2 to 5  $\mu\text{m}$  over about 10 percent of the knife edge), and sparking was observed during the rub. The sparking is thought to be due to the graphite burning.

As a general observation, all of the rub surfaces resulting from interactions with the rotating knife edge were completely or nearly completely smeared with varying degrees of heat discoloration in evidence. Despite the smaller nominal contact area for the knife-edge geometry compared to the blade-tip geometry, radial and frictional loads for the knife-edge tests were not lower than those encountered in the blade-tip tests. With the exception of rub tests against aluminum graphite, temperature peaks of at least 270<sup>o</sup> C were observed at three or four active sites on the knife edge.

#### Survey of Rub Mechanisms and Associated Frictional Energies

Figure 4 indicates the peak frictional heat generation rates per unit nominal contact area for various seal materials evaluated here and in reference 3. These results were calculated from frictional force data in the following manner. The measured values of frictional force were multiplied by an assumed 322 meter per second rub speed in every case (322 m/sec was the rub speed used in ref. 3) no matter what the rub speed during the actual experiment was and then divided by the appropriate nominal contact area. Also, superimposed on the ordinate of figure 4 are ranges of frictional heat generation rate per unit contact area for three distinctly identifiable rub mechanisms: (1) true abrasability, (2) smearing on a low density substrate, and (3) smearing on a dense substrate. A brief description of each mechanism follows with a more detailed treatment included in the appendixes. Figure 5 presents each of the three distinct mechanisms schematically.

True abrasability. - When a gas-path seal material accommodates a rub interaction with the rotor by the mechanism of discrete particle removal with minimal plastic deformation or plowing to the rub surface, it is considered to be truly abrasable. A lower bound to the energy associated with this type of interaction is defined by the total energy required to fracture individual particles out of the rub surface at a rate consistent with the incursion rate of the rotor. Order-of-magnitude calculations in appendix A indicate that this energy is extremely low compared to measured frictional energies as may be seen in figure 4. The process of particle removal is not considered to be very different for the cases of knife-edge or blade-tip rotor geometries.

Extending the individual particle fracture considerations to include effects due to the finite time required for particle removal permits estimating the frictional energy expended over and above that needed only for the fracture process. An estimate of the time required to complete the fracture process for a single particle is given in appendix A. Essentially, the argument amounts to a lower bound estimate of the time required to propagate a crack, growing in a plastic manner, across a typical sinter bond. This time is then used in conjunction with appropriate incursion parameters to estimate the effective contact area during the rub interaction. The frictional energy estimate for this situation (indicated on the ordinate of fig. 4) follows directly using reasonable values of material bulk strength and rub speed.

As shown by figure 4, measured frictional energies for gas-path seal materials that certainly behave as truly abrasable materials (40 percent dense sintered Nichrome and the fibermetal under nonsmearing conditions) do in fact fall in the range of magnitude predicted. The best example of such a material is afforded by the 40-percent-dense sintered Nichrome. That this material may in fact be considered truly abrasable is supported by the micrographs in figure 6. The debris collected after rub interaction (figs. 6(a) and (b)) is seen to consist of discrete sintered particles. The rub surface (fig. 6(c)) shows no evidence of smearing; the particulate nature of the material is still in evidence.

The truly abrasable model developed in appendix A is further supported by comparing the results summarized in figure 2(a) for 40-percent-dense sintered Nichrome and plasma-sprayed nickel graphite with equation (2a) (from appendix A):

$$\dot{Q} = \mu \left( \sigma_{AM} \frac{\dot{\Delta} t'}{\rho^{1/3} d} \right) V$$

The term  $\mu \left[ \sigma_{AM} (\dot{\Delta} t' / \rho^{1/3} d) \right]$  is the predicted friction force per unit contact area. For the tests on sintered Nichrome and plasma-sprayed nickel graphite summarized in figure 2(a), friction loads are on the predicted order (0.06 to 0.3 N/cm<sup>2</sup>), they increase with incursion rate  $\dot{\Delta}$ , and for the sintered Nichrome at least they do not

depend strongly on rub velocity  $V$ .

Smearing on a low density substrate. - Under some conditions, the particles comprising the rub surface of a low density porous gas-path seal material are plastically smeared during the rub interaction. Thus, the rotor encounters a fully dense "paved" rub surface on a low density substrate. Conditions that tend to promote smearing are discussed in a later section.

An order of magnitude estimate of the rate of frictional energy generation when the rotor encounters a smeared surface on a low density substrate is included in appendix B. Contributions due to plastic displacement of seal material in the radial direction and the effects of high sliding speed friction in the direction of rotation are considered. Under typically encountered incursion rates the radial plastic displacement contribution to energy generation is found to be negligible. Sliding friction energy contributions are governed by the effective strength of the low density material under the rub surface. Obviously, as the incursion proceeds the density of the material under the smeared surface increases. This leads to progressive hardening of the substrate and an ever increasing rate of frictional heating.

The measured frictional energy values shown in figure 4 for the case of the smeared fibermetals are in the range of magnitudes predicted. That the fibermetal showed a greater propensity to smear than did sintered Nichrome is perhaps due to the greater difficulty of removing fibermetal particles. The extent of rub surface smearing and subsurface densification for sintered Hastelloy fibermetal is indicated in figures 7(a) to (c). Debris collected from this test is shown in figures 7(d) to (g). Pieces obviously from the smeared surface are mixed with very fine debris particles. Close examination of the fine particles reveals spherical and scroll-like shapes. An X-ray energy dispersion analysis shows that some of the fine particles are from the rotor; that is, the titanium contents were high. Also, the smeared rub surface was found to contain considerable titanium that must have transferred from the rotor.

Blade-tip specimens that had been subjected to rub interactions against the 21.5-percent-dense sintered fibermetal at 115 meters per second, resulting in smearing of the fibermetal, showed considerable effects attributable to frictional heating at the rub surface. Figure 8 shows regions of porosity beneath the blade tip rub surface thought to be due to rapid local oxidation and melting of the Ti-6Al-4V during the rub. The regions around the heat affected areas etched differently from the surrounding blade material. This is believed to be caused by  $\alpha$ -phase stabilization that occurs upon dissolution of quantities of oxygen in the  $\alpha$ - $\beta$  Ti-6Al-4V alloy. It should be remembered that intense white sparking and incandescence in the rub zone accompanied these tests.

Extension of the smeared rub energetics description to the case of increased substrate densification leads to higher predicted frictional energies because of higher radial loads. The porous cermet material shown in figure 4 (evaluated in ref. 3) typifies

this situation with substrate densities of the order of 70 percent. Radial loads are envisioned to be governed by a plastic indentation mechanism for knife-edge rub interaction geometries. The rub groove on dense aluminum (fig. 9) illustrates the plastic indentation mechanism controlling the normal load for a highly dense seal material.

Under some conditions the analog between blade-tip rub interactions against smeared or dense materials and the machining process appears to be quite good. For example, nearly fully dense plasma-sprayed aluminum exhibits a surface finish suggestive of a machining process (see fig. 9(a)). Furthermore, the debris consists mostly of very thin aluminum flakes (fig. 9(b)) as would be generated under extremely low feed rate conditions. Aluminum transfer deposits in the form of thin sheets may be seen on the blade tips in figure 9(c).

### Transitions Observed in the Rub Mechanisms of Gas-Path Seal Materials

It was noted in the rub test results (figs. 2 and 3) that the frictional and normal loads, and particularly the degree of smearing observed on fibermetal materials and NiCr-BN, depended on rub interaction conditions (rub speed, incursion rate, geometry). Also, it was noted that the incidence of smearing of all materials was greater under knife-edge seal geometry tests than under blade-tip geometries. Such dependencies have been seen in other studies (ref. 8), and it is widely observed that gas-path seal performance is dependent on rub interaction parameters and seal geometries. In this section, an attempt is made to model the processes promoting the variation of rub mechanisms with gas-path seal test conditions. Two complementary models are developed. One is based on thermal effects, the other on particulate debris escape effects.

Thermal effect model. - In this model, transition from a porous to a smeared seal material rub surface is envisioned to occur because of thermal softening of the seal material particles due to frictional heating. Hence, an analytical description is developed indicating how the temperature in the seal material might vary as a function of depth beneath the rub surface under varied incursion rate conditions. Thermal effects to the gas-path seal material are modeled by considering the contact surface to be analogous to the surface of a body undergoing ablative material loss. The situation is presented schematically in figure 11. The rub interaction is idealized by assuming a uniform contact surface, steady-state conditions in a moving coordinate system having its origin at the seal rub surface, and one-dimensional heat-transfer effects. The resulting heat-transfer equation (ref. 4) becomes

$$\frac{\partial}{\partial x} \left( K_{SM} \frac{\partial T}{\partial x} \right) = -\dot{\Delta} \bar{\rho} C_p \frac{\partial T}{\partial x} \quad (1)$$

The thermal conductivity of the seal material is given by  $K_{SM}$ ,  $\dot{\Delta}$  is the rate at which the contact surface moves into the seal material, and  $\rho$  and  $C$  are the density and specific heat of the seal material. The boundary conditions are

$$T = T_{cr} \quad \text{at } x = 0$$

$$T = T_{\infty} \quad \text{for large } x$$

where  $T_{cr}$  is a limiting sliding surface temperature and  $T_{\infty}$  the bulk seal material temperature. The value of  $T_{cr}$  is not easily specified, but  $T_{cr}$  may be interpreted as being a lowest thermodynamic heat sink temperature - for example, incipient melting (ref. 5) or a distinct softening temperature resulting from metallurgical transformations such as recrystallization (refs. 6 and 7).

The solution to equation (1) is

$$\frac{T - T_{\infty}}{T_{cr} - T_{\infty}} = \exp\left(-x \dot{\Delta} \frac{\bar{\rho} C_p}{K}\right) \quad (2)$$

and is presented graphically in figure 11. Physically, the rapid introduction of "cold" bulk seal material to the vicinity of the rub interface under high incursion rate (high  $\dot{\Delta}$ ) conditions results in a steep temperature gradient and high heat flux necessary to maintain the rub surface at  $T_{cr}$ . Conversely, high temperature effects are seen to penetrate deeply into the seal material when  $\dot{\Delta}$  (approximately equal to the incursion rate) is low. This is consistent with the observation of increased seal material smearing tendencies observed under low incursion rate conditions. Increased smearing is promoted by thermal softening of the seal material. The effect of incursion rate on smearing for the case of 19-percent-dense fibermetal is summarized in figure 12. Similar trends of increased smearing under low incursion rate conditions were observed for the 21-percent-dense fibermetal and the 40-percent-dense sintered NiCr. This simple thermal effect model has also been proposed to account for rub surface smearing and rotor wear trends under varied incursion rate conditions for knife-edge interactions (ref. 8). Smearing, in effect rub surface densification, is undesirable as it promotes high energy rub interactions, destructively high temperatures, and increased blade-tip wear.

Particle escape model. - This model is particularly applicable to low density porous materials and describes a process whereby rub surface densification results from less than 100-percent escape efficiency of abrasible material particles. Slightly different variations of the model are developed for blade-tip and knife-edge interaction geometries.

A densified zone on a low density seal material rub surface may also be developed if some seal material particles initially ejected become reimbedded. This process may be modeled by simple particle balance considerations:

$$N = \frac{n_i - n_e}{bL}$$

where  $b$  is the rotor (knife edge or blade tip) width,  $L$  the rub length,  $N$  the number of particles imbedded per unit rub area,  $n_i$  the total number of particle/rotor contact events to have occurred at time  $t$ , and  $n_e$  the total number of particles to have escaped from the rub zone at time  $t$ .

At time  $t$  the rate at which particles interact with the rotor is

$$n_i(t) = \frac{bL \dot{\Delta}}{d} \underbrace{\left( \underbrace{\frac{\rho_0}{d^2}}_{\text{initial surface density}} + \underbrace{\frac{n_i - n_e}{bL}}_{\text{total number imbedded}} \right)}_{\text{total surface density at time } t} \quad (4)$$

The term  $\rho_0/d^2$  gives the initial number of particles per unit area present on the rub surface with  $\rho_0$  being the initial density  $\left(1 - \frac{\text{percent porosity}}{100}\right)$  of the material and  $d$  the average particle diameter. The term  $bL \dot{\Delta}/d$  normalizes the incursion rate ( $\dot{\Delta}$ ) with respect to particle size and therefore physically gives a rate at which the particle layers are encountered.

The number of particles to have escaped after rub time  $t$  is sensitive to the rub geometry. For blade-tip geometries the simple assumption is made that a constant fraction of the particles encountered can escape. This gives

$$n_e = C_1 n_i \quad (5)$$

Very likely  $C_1$  is a function of contact length  $L$  and decreases as  $L$  increases. For knife-edge geometries, the continuous nature of the contact is envisaged to control the escape of particles giving

$$n_e = C_2 bt \quad (6)$$

For the case of blade-tip geometries, combining equations (4) and (5) results in

$$\dot{n}_i - n_i \left[ \frac{(1 - C_1)\dot{\Delta}}{d} \right] - \frac{\rho_0 b L \dot{\Delta}}{d^3} = 0 \quad (7)$$

Solving equation (7), with the initial condition that  $n_i = 0$  at  $t = 0$ , gives

$$n_i = \frac{\rho_0 b L}{(1 - C_1) d^2} e^{(1 - C_1)\dot{\Delta}t/d} - \frac{\rho_0 b L}{(1 - C_1) d^2} \quad (8)$$

The surface density at time  $t$ , defined as the fractional surface coverage by seal material particles, may be expressed as the ratio of the rate at which particles are encountered at time  $t$  to the rate at which they would be encountered where the surface fully dense. Thus,

$$\text{Surface density} = \frac{\dot{n}_i(t)}{\frac{bL}{d^2} \frac{\dot{\Delta}}{d}} = \rho_0 e^{(1 - C_1)\dot{\Delta}t/d} \quad (9)$$

gives the surface density at time  $t$ . Three points are of special significance in equation (9). First, the only parameter not known a priori is the escape particle fraction  $C_1$ . Second, surface densification increases very rapidly with rub depth  $\dot{\Delta}t$  and is sensitive to the value of  $C_1$ . Third, rapid surface densification is favored by a fine particle size  $d$ . Figure 13 illustrates some experimental evidence that greater densification does in fact occur in a material with a finer particle size.

Combining equations (4) and (6) for the knife-edge geometry and solving gives

$$n_i = \left( \frac{\rho_0 b L}{d^2} - \frac{C_2 b d}{\dot{\Delta}} \right) e^{\dot{\Delta}t/d} + C_2 b t - \frac{\rho_0 b L}{d^2} + \frac{C_2 b d}{\dot{\Delta}} \quad (10)$$

The surface density for this case may be expressed as

$$\text{Surface density} = \frac{\dot{n}_i(t)}{\frac{bL}{d^2} \frac{\dot{\Delta}}{d}} = \left( \rho_0 - \frac{C_2 d^3}{L \dot{\Delta}} \right) e^{\dot{\Delta}t/d} + \frac{C_2 d^3}{L \dot{\Delta}} \quad (11)$$

The only parameter not known beforehand in equation (11) is  $C_2$ . Now, however, in addition to the exponential dependency on rub depth  $\dot{\Delta}t$ , surface density also increases with increased incursion rate  $\dot{\Delta}$  by virtue of the  $(\rho_0 - C_2 d^3 / L \dot{\Delta})$  coefficient. Fig-



ure 14 shows the smearing tendencies (increased smearing with increased incursion rate) for low density sintered Nichrome under varied knife-edge seal interaction conditions.

## CONCLUSIONS

Experimental evidence and theoretical considerations for various abradable gas-path seal materials under simulated seal rub conditions lead to the following conclusions:

1. The first-order frictional energy generation rates per unit contact area estimates are consistent with experimental results for cases of clearly identifiable seal material wear mode regimes.

2. The friction and wear performance of the gas-path seal materials studied, particularly the low density materials, is seen to be sensitive to incursion rate, rotating velocity, and seal geometry through the occurrence of rub surface densification or smearing.

3. Two models are proposed to describe the mechanisms promoting smearing. One is based on a seal material thermal softening effect, the other on a wear particle escape mechanism. Together they predict enhanced surface densification under extremes of low and high incursion rate conditions when seal material particle size is small and when under knife-edge rub geometries as opposed to blade-tip rub geometries. The predictions are consistent with the experimental evidence at hand.

4. Sintered 40-percent-dense Nichrome and plasma-sprayed nickel - 25 percent graphite are the most rub tolerant of the seal materials investigated.

5. It was shown that providing a low density compliant substrate for the fully dense plasma-sprayed aluminum seal material results in significant reductions in frictional and radial loads.

Lewis Research Center,  
National Aeronautics and Space Administration,  
Cleveland, Ohio, September 20, 1977,  
505-04.

## APPENDIX A

### FRictional Energy Estimates for an Abradable Material

Two calculations are introduced here - one representing the energy required simply to fracture discrete particles off the abradable material surface, the other including frictional effects accompanying the fracture process. These are order-of-magnitude-type calculations intended to show the comparative significance of fracture energy effects and frictional energy effects. It will be shown that the frictional effects totally dominate the energy required solely for fracture.

#### Fracture of Discrete Particles

The bulk of the fracture energy is consumed by plastic dissipation and as shown in reference 9 may be expressed in terms of surface energy  $\gamma_S$ , crack tip radius  $r$ , and Burgers vector  $\bar{b}$  as

$$\gamma_f = 2\gamma_S \frac{r}{\bar{b}}$$

For ductile cracks propagating rapidly,  $r/\bar{b} \approx 10$ .

The fracture surface area per particle is expressed in terms of particle diameter  $d$ , number of sinter bonds per particle  $n$ , and average sinter bond diameter  $d/m$ :

$$A = n \frac{\pi}{4} \frac{d^2}{m^2}$$

The total area of fracture surface generated per unit time per unit rub surface area is given by the rate at which particles are removed for a given incursion rate  $\dot{\Delta}$ , material density  $\rho$  (i. e.,  $1 - \text{porosity}$ ), and particle diameter  $d$ :

$$A_f = \frac{\dot{\Delta}}{\rho d^3} A$$

Total fracture energy per unit rub surface area involved in the incursion is then approximated by

$$\dot{Q}_f = \dot{A}_f \gamma_f = \left( \frac{\dot{\Delta}}{\rho d^3} \right) \left( n \frac{\pi}{4} \frac{d^2}{m^2} \right) \left( 2\gamma_S \frac{r}{\bar{b}} \right) \quad (\text{A1})$$

If, for example,  $\dot{\Delta} = 25.4 \times 10^{-6}$  meter per second,  $d = 50 \times 10^{-6}$  meter,  $\rho = 0.3$ ,  $n = 4$ ,  $r/\bar{b} = 10$ , and  $\gamma_S \approx 10^{-4}$  joule per square centimeter,

$$Q_f \approx 4 \text{ N-m/m}^2\text{-sec} = 2 \times 10^{-3} \text{ ft-lb/in}^2\text{-sec}$$

which is clearly quite low compared to measured levels of frictional energy.

### Frictional Energy for Abradable Materials

Account must be taken of the fact that ductile crack propagation requires a finite length of time and that particles are not removed simply at the rate of geometric interference. A very rough estimate of the time required for this ductile fracture process to occur may be obtained from simple dislocation considerations. Assuming a dynamic dislocation spacing of about  $100\bar{b}$  and a mean effective dislocation velocity of about 1 meter per second (ref. 10), the minimum number of dislocations required to propagate a ductile crack across a sinter bond of diameter  $d/m$  is

$$\eta = \frac{d/m}{\bar{b}} = 4 \times 10^4$$

for  $d = 50 \times 10^{-6}$  meter and  $m = 5$ , as before. Moving 1 meter per second with a separation of  $100\bar{b}$ , the time required for this parade of  $4 \times 10^4$  dislocations to pass is

$$t' = \frac{(\eta)(100\bar{b})}{1 \text{ m/sec}} = 0.8 \times 10^{-3} \text{ sec}$$

This is essentially the time required to generate an abradable particle. The number of particles per unit rub surface area actually suffering an interaction at any instant is

$$N = \frac{\dot{\Delta}}{\rho d^3} t'$$

This may be expressed in terms of the percent of the rub surface area supporting the radial at any instant:

$$A_r = \frac{N}{\frac{1}{\rho^{2/3} d^2}} = \rho^{2/3} d^2 N$$

The radial load per unit rub surface area may be expressed as

$$P = \sigma_{SM} A_r$$

and the rate of frictional energy generation per unit rub surface area is

$$\dot{Q} = \mu PV = \mu \sigma_{SM} \rho^{2/3} d^2 \frac{\dot{\Delta}t'}{\rho d^3} V = \mu \sigma_{SM} V \frac{\dot{\Delta}t'}{\rho^{1/3} d} \quad (A2)$$

For example, if  $\sigma_{SM} = 12 \times 10^6$  newtons per square meter,  $\mu = 0.3$ ,  $V = 322$  meters per second,  $\rho = 0.3$ , and  $d = 50 \times 10^{-6}$  meter,

$$\dot{Q} = 1.4 \times 10^6 \frac{\text{N-m}}{\text{m}^2\text{-sec}} \approx 650 \text{ ft-lb/in}^2\text{-sec}$$

Clearly the rate of frictional heat generation per unit rub surface area dominates the fracture energy requirement.

## APPENDIX B

### SMEARING ON A LOW DENSITY SUBSTRATE

There are two contributions to heat generation associated with rub interactions when a thin, smeared layer forms on a porous substrate. First, there is plastic energy dissipated in the seal material due to normal plunge (radial incursion) effects. For thin smeared layers this is significant only in the case of knife-edge interactions. This heat contribution (ref. 11) may be expressed as

$$Q_P = \frac{2.6}{2 \left( H + \frac{b}{2} \right)} \dot{\Delta} \sigma_y H$$

where  $H$  is the smeared layer thickness,  $\sigma_y$  the fully dense flow stress of the seal material, and  $W$  the knife-edge width. Under conditions in which the abradable material approaches full density throughout, the previous relation becomes applicable to blade-tip interactions. For the case in which  $\dot{\Delta} = 25.4 \times 10^{-6}$  meter per second,  $\sigma_y = 16 \times 10^7$  newtons per square meter, and  $H = 254 \times 10^{-6}$  meter,

$$\dot{Q} = 80 \text{ N-m/m}^2\text{-sec} \approx 0.04 \text{ ft-lb/in}^2\text{-sec}$$

It is apparent that this contribution can be significant only if  $\dot{\Delta}$  is very large and/or the densified layer and contact width become very thick.

The second contribution to heat generation for the case of smearing is direct frictional heating. This is expressed by

$$\dot{Q} = \mu \sigma_{AM} V$$

where  $\sigma_{AM}$  is the substrate (low density material) hardness or yield strength. Under high velocity sliding conditions typical of gas-path seal rub interactions dynamic softening of the smeared layer is anticipated. This will be particularly significant here as the low density substrate is a poor thermal conductor and frictional energy dissipated in the smeared layer is not efficiently removed. Under these conditions low friction is usually observed. If a friction coefficient of 0.1 is assumed and the low density material has a strength level of about  $12 \times 10^6$  newtons per square meter at a 322 meter per second (1000 ft/sec) sliding speed,

$$\dot{Q} = 3.9 \times 10^8 \text{ N-m/m}^2\text{-sec} \approx 1.8 \times 10^5 \text{ ft-lb/in}^2\text{-sec}$$

This quite high value of frictional heat generation is an upper bound to the smeared rub condition in the sense that 100 percent smearing and uniform contact over the entire apparent rub surface are tacitly assumed. Densification of the substrate (fig. 5(c)) would manifest itself in an increase in  $\sigma_{AM}$  and larger values of  $\dot{Q}$ .

## APPENDIX C

### SYMBOLS

$A_f$	fracture surface area, $m^2$
$b$	width of rub surface, $m$
$\bar{b}$	Burgers vector, $m$
$C_p$	specific heat, $J/kg-^{\circ}C$
$C_1$	particle escape fraction for blade tip geometries, dimensionless
$C_2$	particle escape constant for knife-edge geometries, $m\text{-sec}^{-1}$
$d$	particle diameter, $m$
$H$	smeared layer thickness, $m$
$K_{SM}$	thermal conductivity of the seal material, $J/m\text{-sec-}^{\circ}C$
$L$	length of rub surface, $m$
$m$	ratio of bond diameter to particle diameter
$N$	number of particles imbedded in rub surface per unit area, $m^{-2}$
$n$	number of interparticulate bonds per particle
$n_e$	number of particles that escape from rub surface
$n_i$	number of particles interacted with during rub interaction
$\dot{Q}$	rate of frictional energy generation per unit contact area, $J/m^2\text{-sec}$
$r$	radius of crack tip, $m$
$T$	temperature, $K$
$t$	time (independent variable), $sec$
$t'$	time required to remove a discrete particle, $sec$
$V$	sliding velocity, $m/sec$
$\gamma_f$	work of fracture, $J/cm^2$
$\gamma_s$	surface energy, $J/cm^2$
$\dot{\Delta}$	incursion rate, $m/sec$
$\mu$	coefficient of friction

$\rho$	particulate density (i. e. , 1 - porosity), dimensionless
$\bar{\rho}$	mass density, $\text{kg/m}^3$
$\sigma_{\text{SM}}$	strength (hardness) of seal material, $\text{N/m}^2$
$\sigma_y$	yield strength of full dense seal material, $\text{N/m}^2$



## REFERENCES

1. Roelke, Richard J.: Miscellaneous Losses. Turbine Design and Application, Arthur J. Glassman, ed., NASA SP-290, 1973, pp. 125-148.
2. Hauser, Cavour H.; et al.: Compressor and Turbine Technology. Aeronautical Propulsion. NASA SP-381, 1975, pp. 229-288.
3. Shiembob, L. T.: Development of Abradable Gas Path Seals. (PWA-TM-5081, Pratt and Whitney Aircraft; NASA Contract NAS3-18023.) NASA CR-134689, 1974.
4. Rohsenow, Warren M.; and Choi, Harry Y.: Heat, Mass, and Momentum Transfer. Prentice Hall, Inc., 1961, p. 122.
5. Ho, Ting-Long: Some Wear Studies on Aircraft Brake Systems. (Rensselaer Polytechnic Inst.; NASA Grant NGR 33-018-152.) NASA CR-134989, 1975.
6. Bill, Robert C.; and Wisander, Donald: Recrystallization as a Controlling Process in the Wear of Some F. C. C. Metals. Wear, vol. 41, 1977, pp. 351-363.
7. Barker, K.; et al.: Cyclic Wear Behavior Produced by Thermal Metallurgical and Chemical Action. Presented at the ASLE 32nd Annual Meeting (Montreal, Quebec), May 9-12, 1977.
8. Bill, Robert C.; and Shiembob, Lawrence T.: Friction and Wear of Sintered Fibermetal Abradable Seal Materials. NASA TM X-73650, 1977.
9. Averbach, B. L.; et al., eds.: Fracture: Proceedings of an International Conference on the Atomic Mechanisms of Fracture. (Swampscott, Mass.), Apr. 12-16, 1959. Technology Press of MIT, 1959, p. 513.
10. Cottrell, Alan Howard: Dislocations and Plastic Flow in Crystals. Clarendon Press (London), 1953, p. 66.
11. Rowe, Geoffrey W.: Principles of Metalworking. St. Martins Press, Inc., 1965, p. 83.

TABLE I. - SUMMARY OF RUB DATA

Material	Tip speed, m/sec	Incursion rate, m/sec	Characteristics of radial and frictional load patterns	Rub surface condition after test	Incidence of sparking
Blade tip					
40-Percent-dense sintered Nichrome	57	$25.4 \times 10^{-6}$	Several distinct events, 0.1- to 0.5-sec duration	Cleanly abraded	Occasional yellow sparks
	57	254	Three distinct events, 0.5-sec duration	Cleanly abraded	Occasional yellow sparks
	115	25.4	Several distinct events, 0.1- to 0.5-sec duration	Cleanly abraded	Occasional yellow sparks
Plasma-sprayed nickel - 25 percent graphite	57	$25.4 \times 10^{-6}$	Several distinct events, 0.1- to 0.5-sec duration	Cleanly abraded	Occasional yellow sparks
	57	254	Two distinct events, 0.5- to 1-sec duration	Cleanly abraded	Occasional yellow sparks
	115	25.4	Several distinct events, 0.1- to 0.5-sec duration	Cleanly abraded	Occasional yellow sparks
19-Percent-dense sintered Hastelloy-X fibermetal	57	$25.4 \times 10^{-6}$	Continuous	Smearred over 20 percent of surface	Intermittent bursts of white sparks
	57	254	Continuous for 2 sec with 1 intense event	Frictional tearing observed	Intermittent bursts of white sparks
	115	25.4	Continuous for first 5 sec followed by several distinct events, 0.5- to 1-sec duration	Smearred over 40 percent of surface	Intermittent bursts of white sparks
21.5-Percent-dense sintered Hastelloy-X fibermetal	57	$25.4 \times 10^{-6}$	Continuous with occasional peaks about two times continuous load	Smearred over 10 percent of surface	Intermittent bursts of white sparks
	57	254	Continuous (1- to 2-sec event)	Frictional tearing observed with smearing over 10 percent of surface	Intermittent bursts of white sparks
	115	25.4	Continuous with several peaks about 50 percent higher than continuous load	Smearred over 70 percent of surface	Continuous white incandescence with red glow on rub surface
Plasma-sprayed Nichrome - boron nitride	57	$25.4 \times 10^{-6}$	Continuous with two intense events, 0.1-sec duration	Smearred over 50 percent of surface	Intermittent sparking with red glow on rub surface
	57	254	One intense event, 0.5-sec duration	Smearred ridges; frictional tearing	-----
	115	25.4	One intense event, 4-sec duration	Smearred over 70 percent of surface; frictional tearing	Intense white incandescence
Plasma-sprayed aluminum	115	$25.4 \times 10^{-6}$	Continuous	Smoothly machined surface	No sparking seen
Plasma-sprayed aluminum on 15-percent-dense sintered nickel fibermetal	115	$25.4 \times 10^{-6}$	Continuous	Smoothly machined surface	No sparking seen

Knife edge					
40- Percent-dense sintered Nichrome	115	$25.4 \times 10^{-6}$	Several distinct events	Smearred with heat discoloration	Intermittent sparking with incandescence
Plasma-sprayed nickel - 25 percent graphite	115	$25.4 \times 10^{-6}$	Several distinct events	Smearred	Intermittent sparking
19- Percent-dense sintered Hastelloy-X fibermetal	115	$25.4 \times 10^{-6}$	Continuous	Smearred with heat discoloration	Sparking with incandescence
21.5- Percent-dense sintered Hastelloy-X fibermetal	115	$25.4 \times 10^{-6}$	Several distinct events	Smearred with heat discoloration	Intense sparking with incandescence
Plasma-sprayed aluminum <sup>a</sup>	115	$25.4 \times 10^{-6}$	Continuous	Plastically displaced material around edge of rub groove	No sparking
Plasma-sprayed aluminum on fibermetal <sup>a</sup>	115	$25.4 \times 10^{-6}$	Continuous	Plastically displaced material around edge of rub groove with recession due to substrate compliance	No sparking
Plasma-sprayed aluminum graphite	115	$25.4 \times 10^{-6}$	Several distinct events	Smearred	Yellow sparking

<sup>a</sup>Tested against 17-4 PH steel knife-edge.

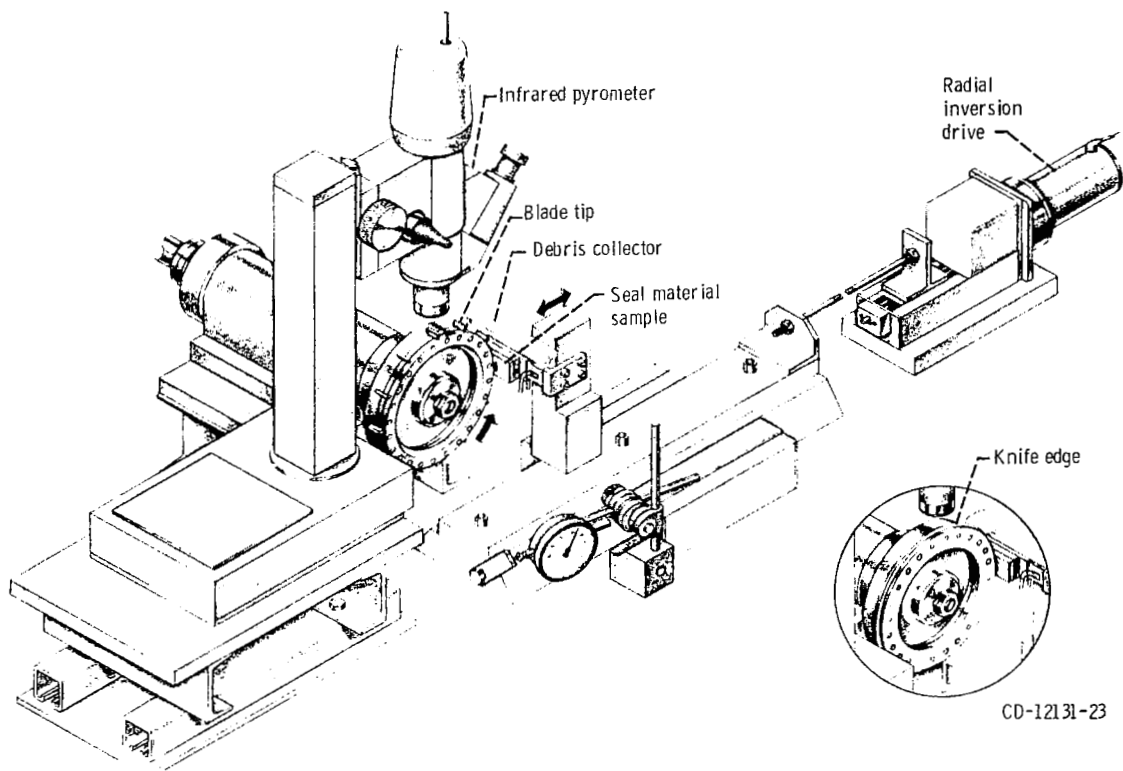
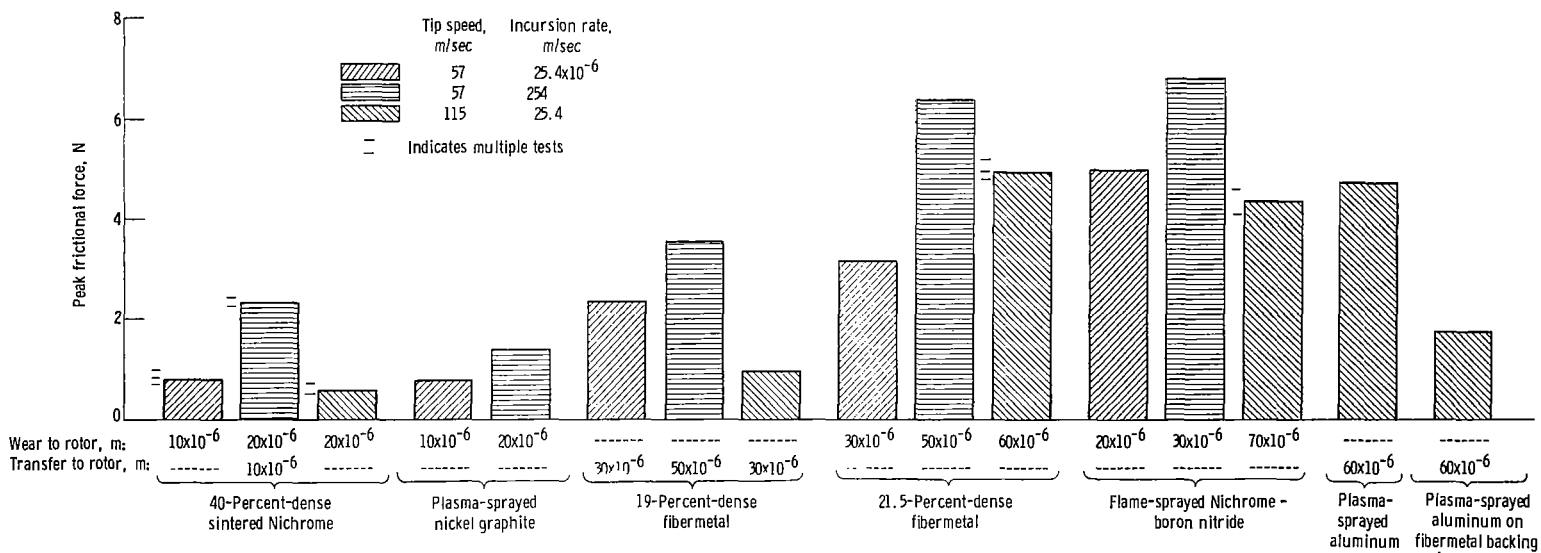
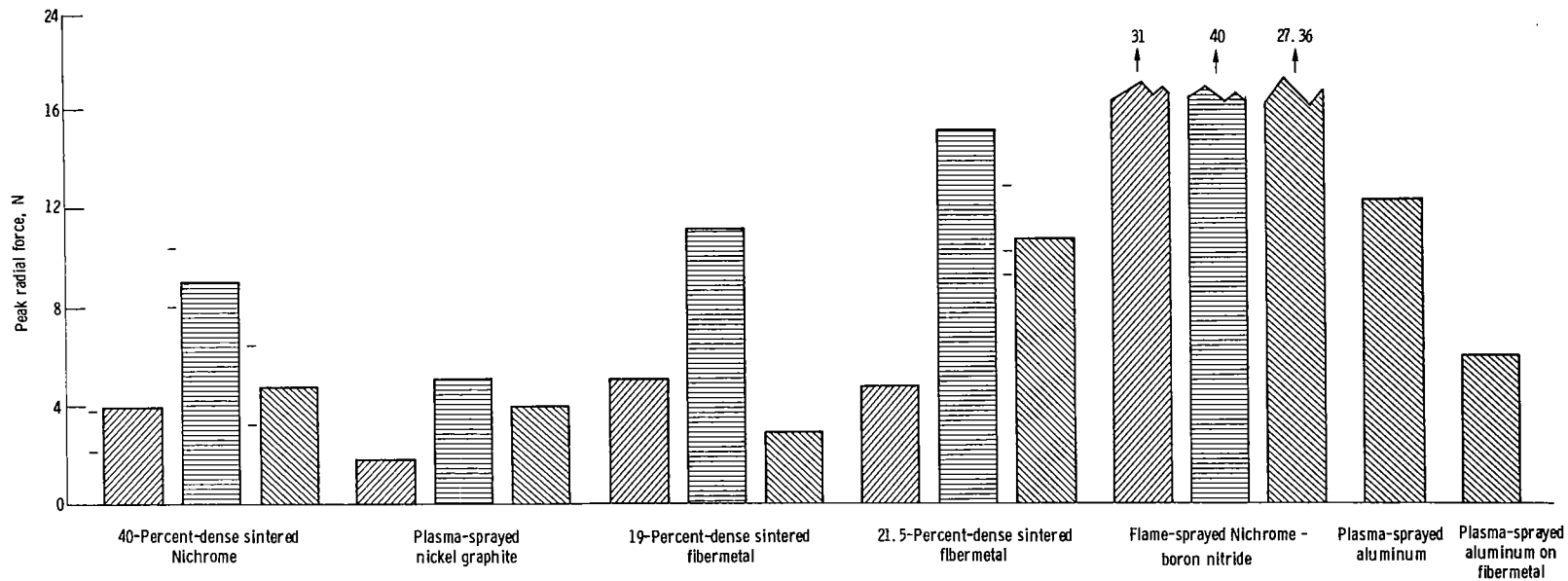


Figure 1. - Test apparatus.



(a) Frictional forces and wear.

Figure 2. - Frictional forces, radial forces, and wear to blade-tip edges for various gas-path seal materials in contact with Ti-6Al-4V blade tips.



(b) Radial forces.  
Figure 2. - Concluded.

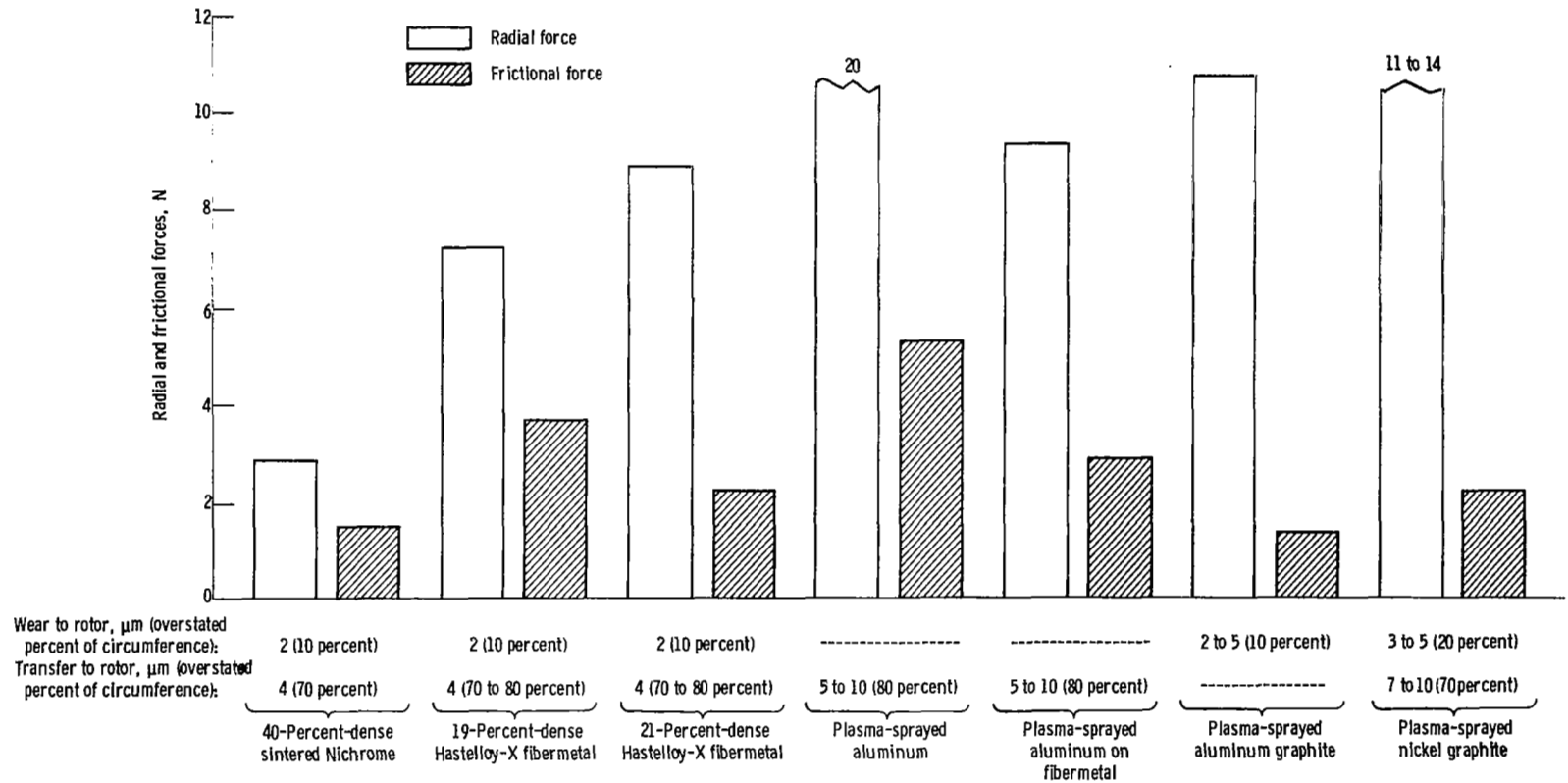


Figure 3. - Frictional and radial loads and rotor wear and transfer for various gas-path seal materials in contact with a FI-6AI-4V labyrinth seal knife edge.

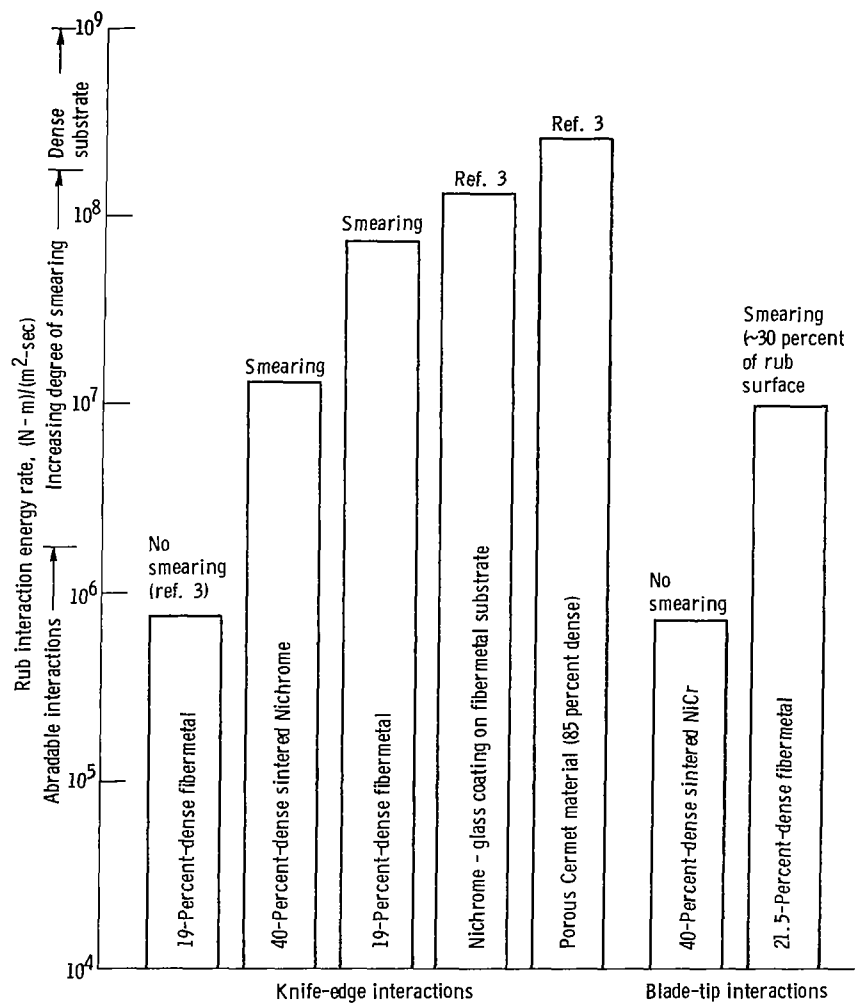
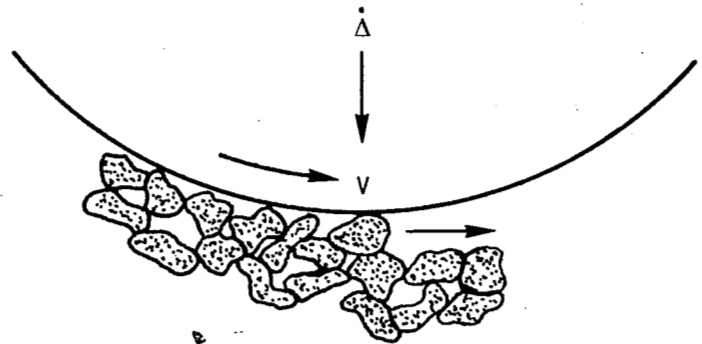
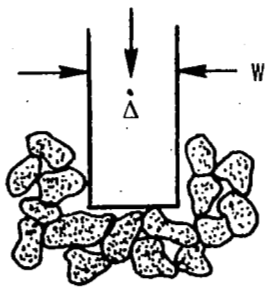
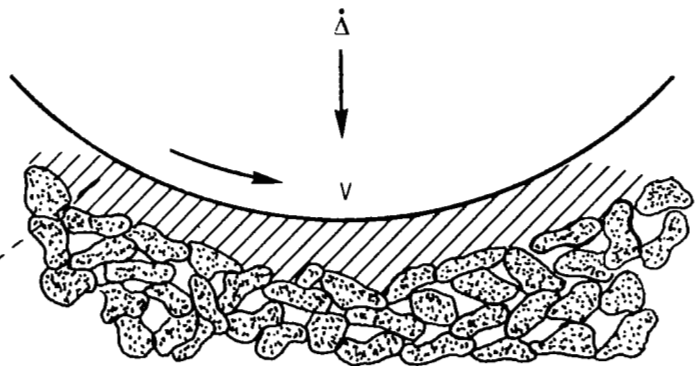
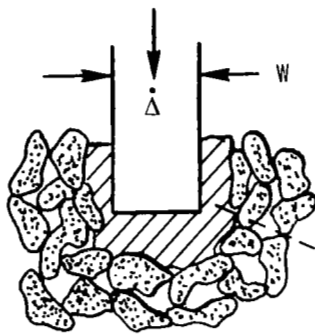


Figure 4. - Rub energy generation rate per unit contact area normalized to a 310 meter per second tip speed for various gas-path seal materials. Different rub conditions result in varied degrees of smearing and subsurface densification.



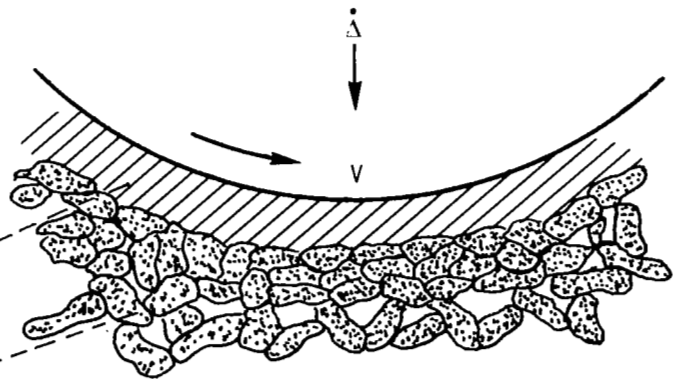
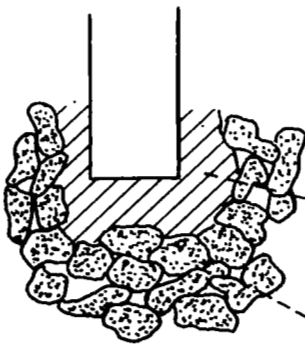


(a) Truly abradable interaction.



Smear layer

(b) Smearing on low density substrate.

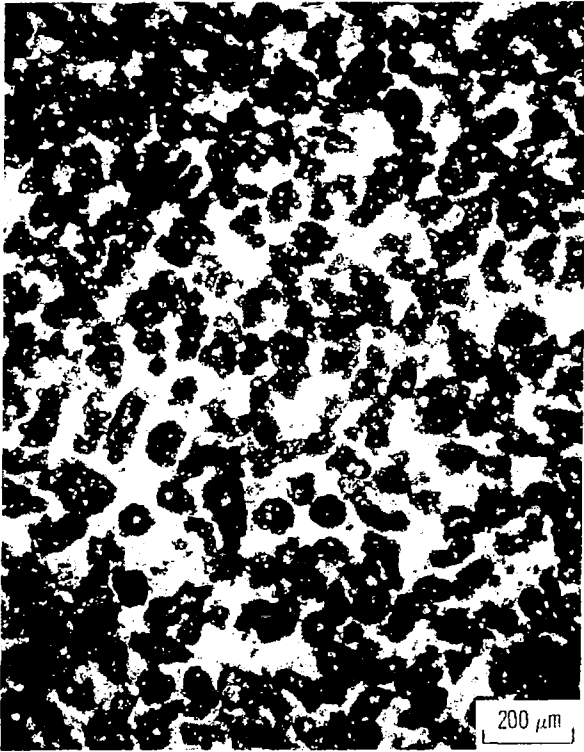


Smear layer

Densified layer

(c) Smearing with densification.

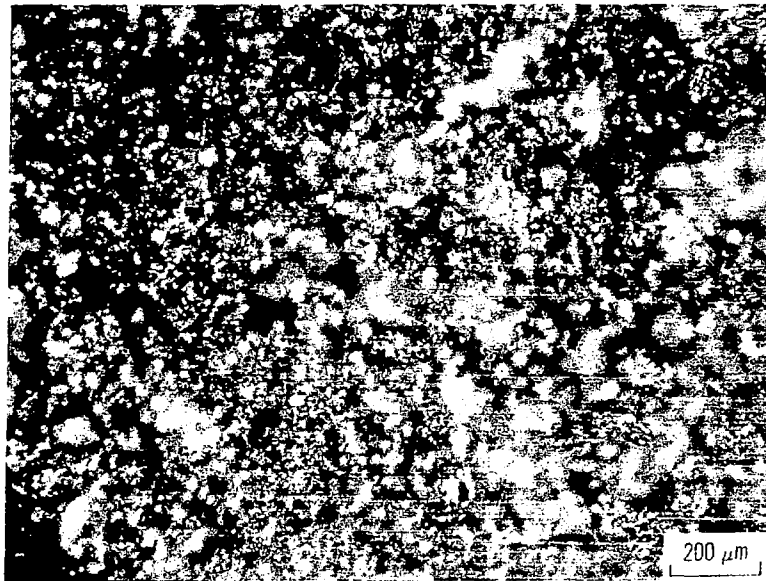
Figure 5. - Schematic representation of various modes of rub interaction between rotor, with peripheral speed  $V$ , driven into a porous gas path seal material at incursion rate  $\Delta$ .



(a) Rub debris.

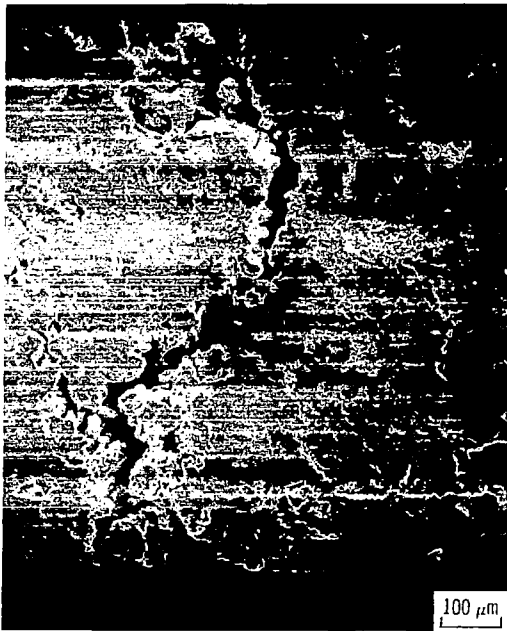


(b) Typical large debris particle showing fracture sites.



(c) Rub surface revealing particulate nature of material.

Figure 6. - Sintered Nichrome debris and rub surface features resulting from interaction with Ti-6Al-4V blade tips.



(a) Rub surface.

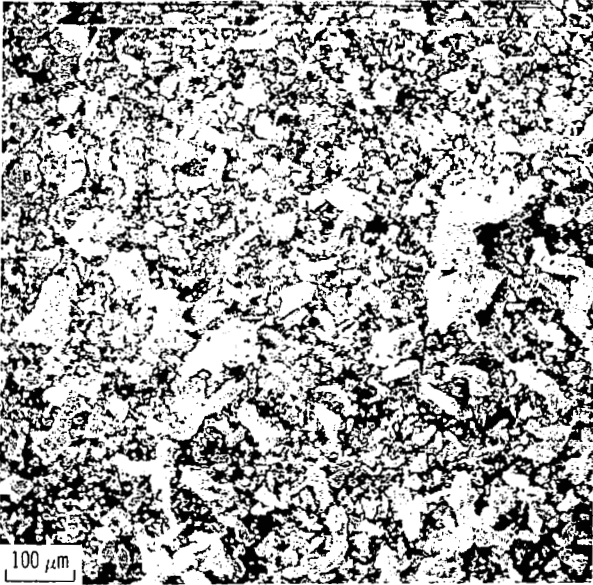


(b) Section through rub groove parallel to sliding direction.



(c) Section through rub groove normal to sliding direction near edge

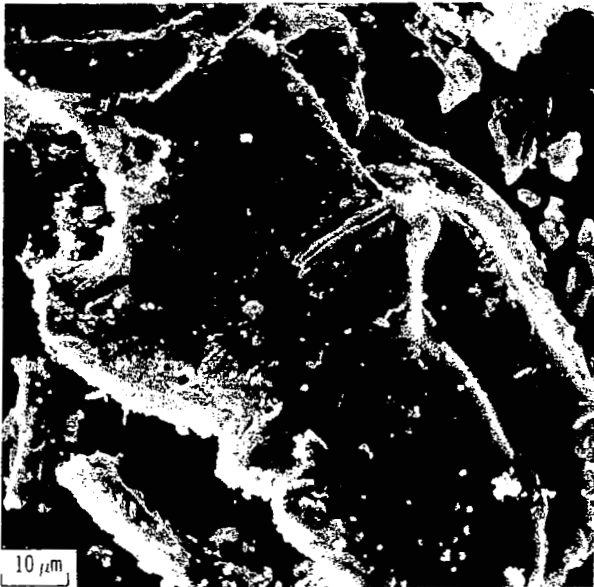
Figure 7. - Rub groove surface and section features observed on sintered Hastelloy-X fibermetal (21.5 percent dense) after rub interaction with Ti-6Al-4V blade tips. Tip speed, 115 meters per second; incursion rate,  $25.4 \times 10^{-6}$  meter per second.



(d) Overview of debris.



(e) Layered particle showing rub surface distress.

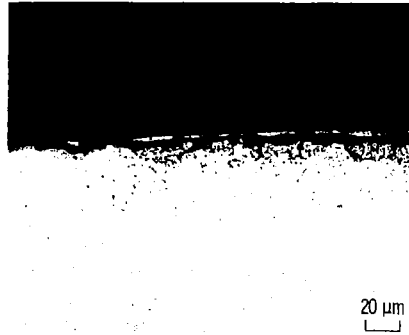


(f) Particle showing chip formation.

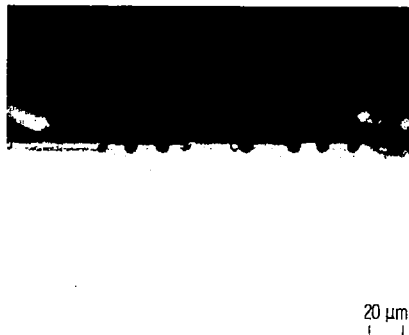


(g) Closeup of "chip" formation.

Figure 7. - Concluded.



(a) Near blade-tip leading edge.



(b) About halfway across blade tip.

Figure 8. - Section view of Ti-6Al-4V blade tip after rub interaction with 21.5-percent-dense Hastelloy-X fibermetal. Tip speed, 115 meters per second; incursion rate,  $25.4 \times 10^{-6}$  meter per second; section plane parallel to direction of sliding.

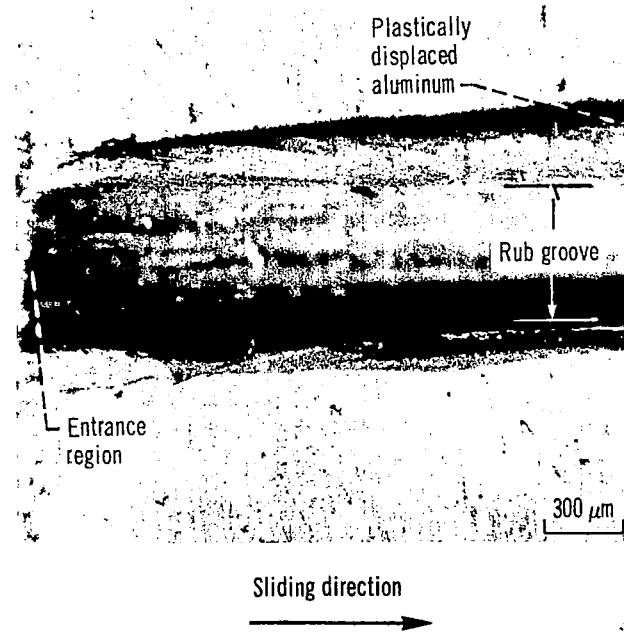
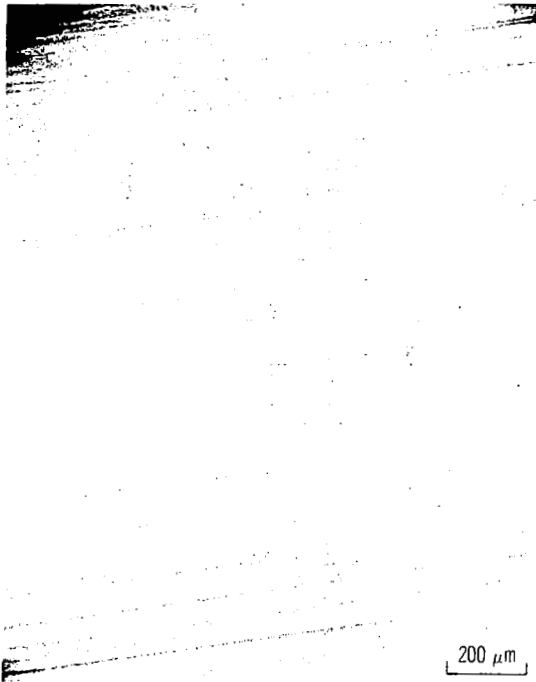
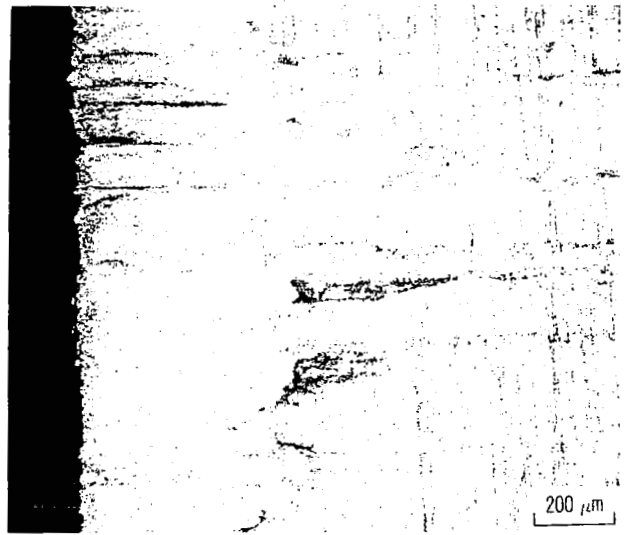


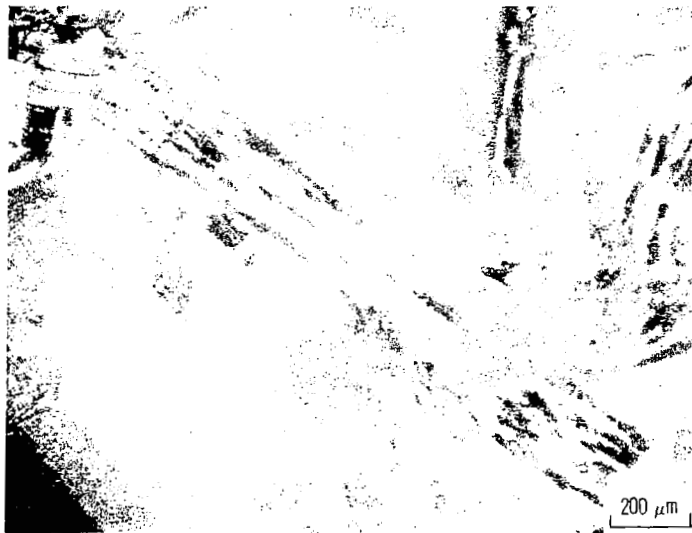
Figure 9. - Rub groove on dense plasma-sprayed aluminum resulting from interaction with Ti-6Al-4V knife edge. Peripheral speed, 115 meters per second; incursion rate,  $25.4 \times 10^{-6}$  meter per second; raised material produced by plastic indentation effect.



(a) Rub surface on plasma sprayed aluminum.



(b) Ti-6Al-4V blade-tip leading edge showing 20 micrometer aluminum transfer.



(c) Wear debris in form of thin translucent ribbons.

Figure 10. - Plasma-sprayed aluminum rub surface, Ti-6Al-4V blade tip, and wear debris resulting from 115 meter per second peripheral speed and  $25.4 \times 10^{-6}$  meter per second incursion rate rub conditions.

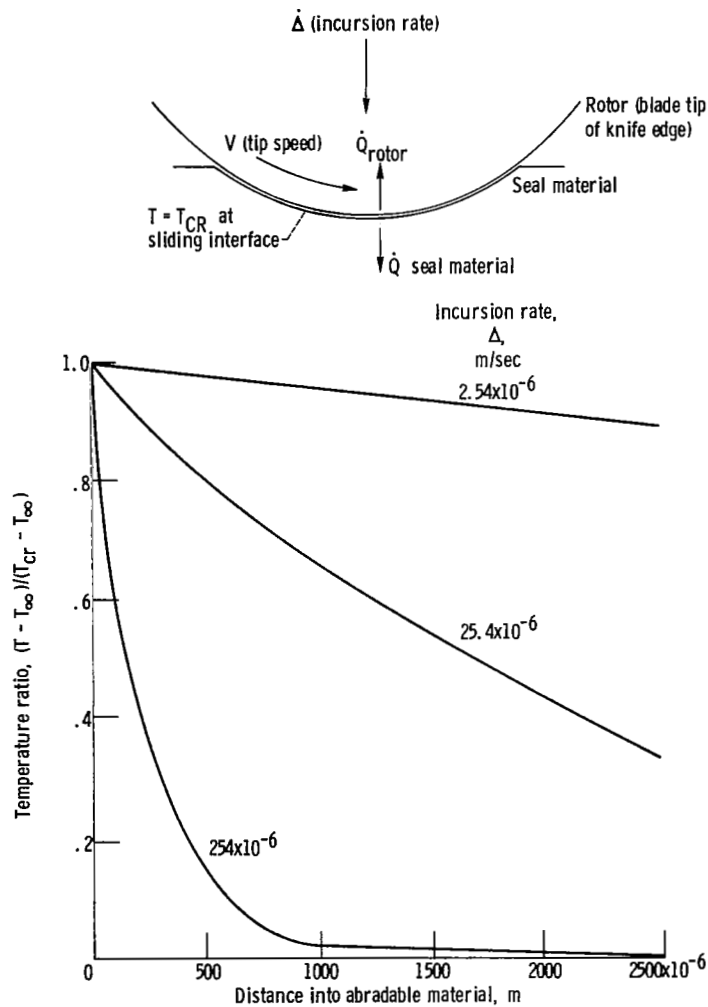


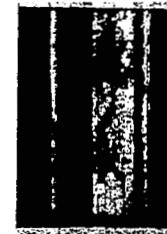
Figure 11. - Schematic representation of temperature profile beneath rub surface, in abradable material.



(a) Tip speed, 57 meters per second; incursion rate,  $254 \times 10^{-6}$  meter per second.

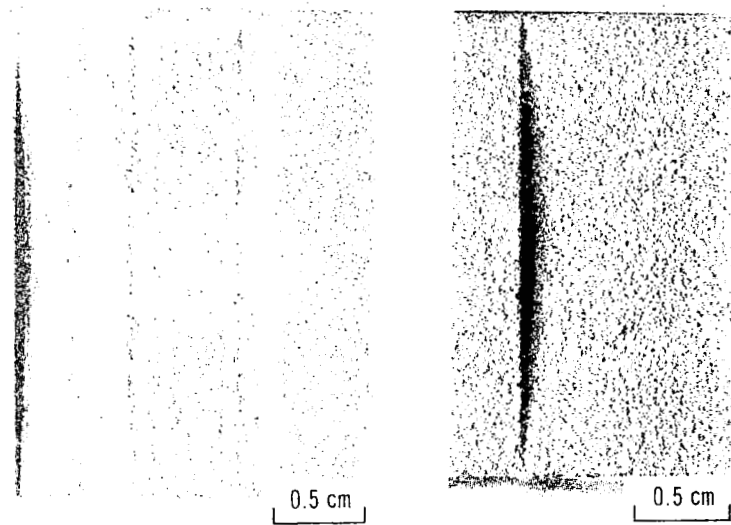


(b) Tip speed, 57 meters per second; incursion rate,  $25.4 \times 10^{-6}$  meter per second.



(c) Tip speed, 115 meters per second; incursion rate,  $25.4 \times 10^{-6}$  meter per second.

Figure 12. - Relative incidence of surface smearing on 19-percent-dense fibermetal under various rub conditions against Ti-6Al-4V blade tips.

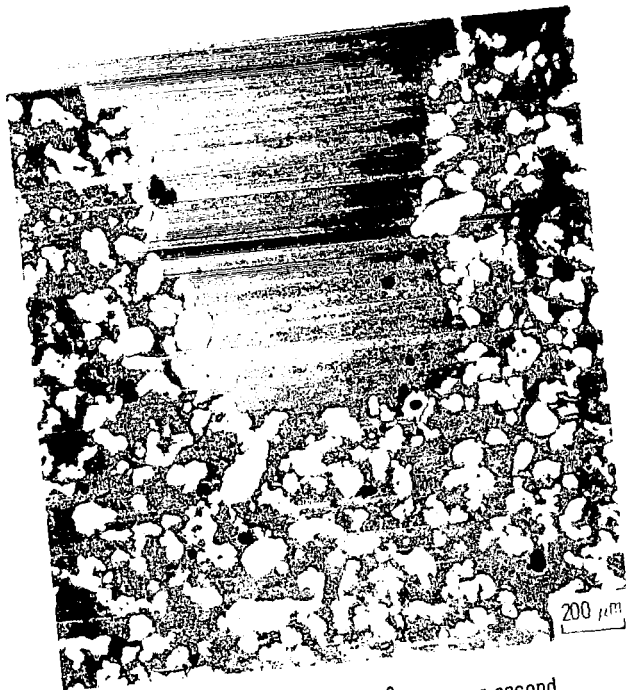


(a) Particle size material, 10 to 20 micrometers.

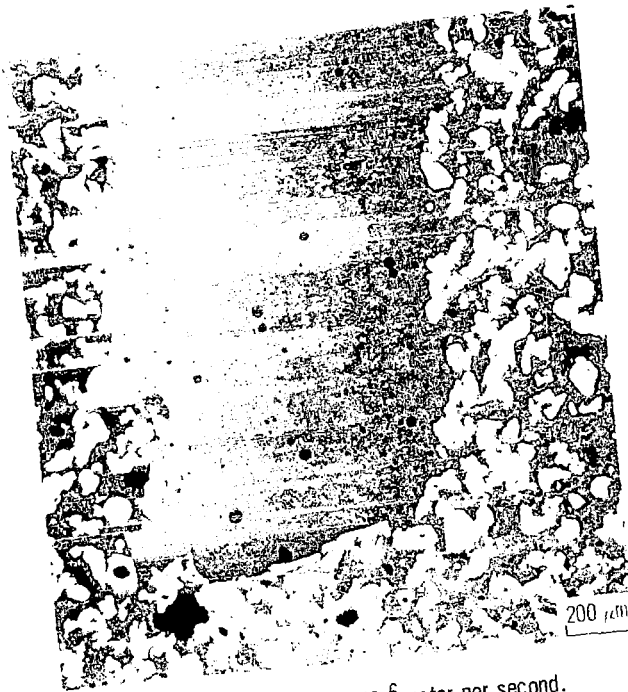
(b) Particle size material, 75 to 100 micrometers.

Figure 13. - Relative incidence of surface smearing on 40-percent-dense sintered Nichrome after rub interaction with Ti-6Al-4V blade tips at 115 meter per second tip speed and  $25.4 \times 10^{-6}$  meter per second incursion rate.





(a) Incursion rate,  $25.4 \times 10^{-6}$  meter per second.



(b) Incursion rate,  $76.2 \times 10^{-6}$  meter per second.



(c) Incursion rate,  $25.4 \times 10^{-6}$  meter per second.

Figure 14. - Rub groove sections after interaction with knife edge at 115 meter per second peripheral speed under indicated incursion rate conditions. Seal material is 40-percent-dense sintered Nichrome.

1. Report No. IP-1128	2. Government Accession No.	3. Recipient's Catalog No.	
4. Title and Subtitle <b>FRICION AND WEAR OF SEVERAL COMPRESSOR GAS-PATH SEAL MATERIALS</b>		5. Report Date January 1978	
		6. Performing Organization Code	
7. Author(s) Robert C. Bill and Donald W. Wisander		8. Performing Organization Report No. E-9276	
		10. Work Unit No. 505-04	
9. Performing Organization Name and Address NASA Lewis Research Center and Propulsion Laboratory U. S. Army R&T Laboratories (AVRADCOM) Cleveland, Ohio 44135		11. Contract or Grant No.	
		13. Type of Report and Period Covered Technical Paper	
12. Sponsoring Agency Name and Address National Aeronautics and Space Administration Washington, D.C. 20546		14. Sponsoring Agency Code	
		15. Supplementary Notes	
16. Abstract <p>Rub interaction experiments were conducted on a series of sintered and plasma-sprayed compressor gas-path seal materials in contact with Ti-6Al-4V blade-tip and knife-edge rotors. The most rub tolerant materials investigated were sintered Nichrome (~40 percent dense) and plasma-sprayed nickel - 25 percent graphite. The effectiveness of providing a compliant substrate for dense seal material coatings was also demonstrated. In general, it was observed that rotor wear and high frictional energy generation rates accompanied smearing or surface densification of the materials investigated. The onset of smearing was sensitive to rub interaction parameters and seal geometry. Two complementary models are proposed to account for the smearing trends. One is based on thermal effects, the other on particulate escape effects. They are shown to be consistent with the experimental evidence at hand, and together they predict that smearing, with the onset of high energy rub conditions, is favored when incursion rates (radial motion) are low, incursion depths are high, the seal geometry is of a knife-edge character, and the seal particle size is small.</p>			
17. Key Words (Suggested by Author(s)) Compressor gas-path seals; Abradable seals; Friction; Wear; Frictional energy; Sintered metal; Plasma-sprayed materials		18. Distribution Statement Unclassified - unlimited STAR Category 26	
19. Security Classif. (of this report) Unclassified	20. Security Classif. (of this page) Unclassified	21. No. of Pages 40	22. Price* A03

\* For sale by the National Technical Information Service, Springfield, Virginia 22161

National Aeronautics and  
Space Administration

THIRD-CLASS BULK RATE

Postage and Fees Paid  
National Aeronautics and  
Space Administration  
NASA-451



Washington, D.C.  
20546

Official Business  
Penalty for Private Use, \$300

9 1 10, C, 121277 S00903DS  
DEPT OF THE AIR FORCE  
AF WEAPONS LABORATORY  
ATTN: TECHNICAL LIBRARY (SUL)  
KIRTLAND AFB NM 87117



POSTMASTER: If Undeliverable (Section 158  
Postal Manual) Do Not Return

S